Nonseismic Signals in the Ocean: Indicators of Deep Sea and Seafloor Processes on Ocean-Bottom Seismometer Data

E. Batsi, E. Tsang-Hin-Sun, F. Klingelhoefer, G. Bayrakci, E.T.Y. Chang, J.-Y. Lin, D. Dellong, C. Monteil, L. Géli

▶ **To cite this version:**

E. Batsi, E. Tsang-Hin-Sun, F. Klingelhoefer, G. Bayrakci, E.T.Y. Chang, et al.. Nonseismic Signals in the Ocean: Indicators of Deep Sea and Seafloor Processes on Ocean-Bottom Seismometer Data. Geochemistry, Geophysics, Geosystems, 2019, 20 (8), pp.3882-3900. 10.1029/2019GC008349 . hal-02944463

HAL Id: hal-02944463
https://hal.science/hal-02944463v1

Submitted on 12 Apr 2021

HAL is a multi-disciplinary open access archive for the deposit and dissemination of scientific research documents, whether they are published or not. The documents may come from teaching and research institutions in France or abroad, or from public or private research centers.

L'archive ouverte pluridisciplinaire **HAL**, est destinée au dépôt et à la diffusion de documents scientifiques de niveau recherche, publiés ou non, émanant des établissements d'enseignement et de recherche français ou étrangers, des laboratoires publics ou privés.

Check for updates

Geochemistry, Geophysics, Geosystems

RESEARCH ARTICLE
10.1029/2019GC008349

Key Points:
- Short-duration high-amplitude events routinely recorded on marine seismometers are not created by fish bumping into the geophone
- In laboratory experiments, the waveforms of these events are well reproduced by fluid migration in the sediments
- We propose three simple source parameters to discriminate gas-related short-duration events in OBS data

Supporting Information:
- Supporting Information S1

Correspondence to:
F. Klingelhoefer,
fklingel@ifremer.fr

Citation:
Batsi, E., Tsang-Hin-Sun, E., Klingelhoefer, F., Bayrakci, G., Chang, E. T. Y., Lin, J.-Y., et al. (2019). Nonseismic signals in the ocean: Indicators of deep sea and seafloor processes on ocean-bottom seismometer data. *Geochemistry, Geophysics, Geosystems*, *20*, 3882–3900. https://doi.org/10.1029/2019GC008349

Received 26 MAR 2019
Accepted 9 JUL 2019
Accepted article online 18 JUL 2019
Published online 5 AUG 2019

©2019. American Geophysical Union. All Rights Reserved.

Nonseismic Signals in the Ocean: Indicators of Deep Sea and Seafloor Processes on Ocean-Bottom Seismometer Data

Evangelia Batsi[1], Eve Tsang-Hin-Sun[1], Frauke Klingelhoefer[1], Gaye Bayrakci[2], Emmy T.Y. Chang[3], Jing-Yi Lin[4,5], David Dellong[1], Clément Monteil[1], and Louis Géli[1]

[1]Marine Geosciences, Ifremer, Plouzané, France, [2]Ocean and Earth Science, National Oceanography Centre Southampton, University of Southampton, Southampton, UK, [3]Institute of Oceanography, National Taiwan University, Taipei, Taiwan, [4]Department of Earth Sciences, National Central University, Taoyuan City, Taiwan, [5]Center for Environmental Studies, National Central University, Taoyuan City, Taiwan

Abstract Ocean-bottom seismometers (OBSs) commonly record short-duration events (SDEs) that could be described by all of these characteristics: (i) duration <1 s, (ii) one single-wave train with no identified *P* nor *S* wave arrivals, and (iii) a dominant frequency usually between 4 and 30 Hz. In many areas, SDEs have been associated with gas- or fluid-related processes near cold seeps or hydrothermal vents, although fish bumps, instrumental, or current-generated noise have been proposed as possible sources. In order to address some remaining issues, this study presents results from in situ and laboratory experiments combined with observations from two contrasting areas, the Sea of Marmara (Turkey) and the Chilean subduction zone. The in situ experiment was conducted at the European Multidisciplinary Seafloor and water column Observatory-Molène submarine observatory (near Brest, France) and consisted in continuously monitoring two OBSs with a camera. The images revealed that no fish regularly bumped into the instruments. Laboratory experiments aimed at reproducing SDEs' waveforms by injecting air or water in a tank filled by sand and seawater and monitored with an OBS. Injecting air in the sediments produced waveforms very similar to the observed SDEs, while injecting air in the water column did not, constraining the source of SDEs in the seafloor sediments. Finally, the systematic analysis of two real data sets revealed that it is possible to discriminate gas-related SDEs from biological or sea state-related noise from simple source parameters, such as the temporal mode of occurrence, the back azimuth, and the dominant frequency.

Plain Language Summary Ocean-bottom seismometers are instruments deployed on the ocean floor to study earthquakes and other sources of noise. They can record large teleseismic earthquakes, like all seismometers, and more specifically smaller submarine earthquakes. However, they also record noise generated by volcanoes, anthropogenic, or biological activity (whale calls). In particular, short events, lasting less than a second, have been reported worldwide with similar characteristics but their origin is still debated. They have been interpreted as fish hitting the instrument, signals generated by hydrothermal activity or by gas expelled out of the sediments. Here, we continuously monitored ocean-bottom seismometers with a camera and show that no fish accidentally stroke the instruments. Then, during laboratory experiments we demonstrate that gas expelled out of the marine sediments into the water can produce short signals very similar to those recorded by the seismometers in real conditions. Finally, we analyzed data from two experiments, one in the Sea of Marmara and the other offshore Chile. We show that short events are generated by gas expelled into the water. This study thus demonstrates the use of marine seismometers to monitor processes related to gas in the sea, which has direct impacts for better quantifying natural risks.

1. Introduction

1.1. Short-Duration Events

Short-period ocean-bottom seismometers (OBSs) traditionally record earthquakes and tectonic or volcanic signals from the seafloor but commonly record numerous nonseismic signals as well. In particular, the occurrence of short-duration events (SDEs) has been reported worldwide and with different types of instruments. Compiling the observations from several studies all over the world (e.g., Buskirk et al., 1981; Diaz et al., 2007; Franek et al., 2017; Hsu et al., 2013; Ostrovsky, 1989; Tary et al., 2012; Tsang-Hin-Sun

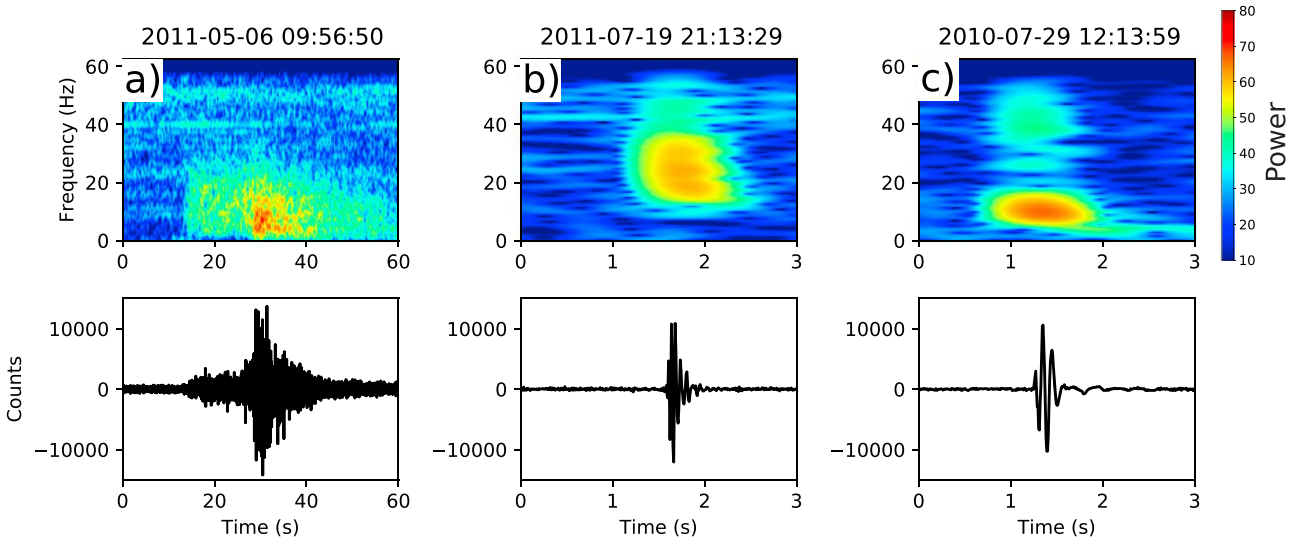

Figure 1. Spectrogram (top panels) and seismogram (bottom panels) of (a) a local earthquake recorded in the Sea of Marmara (Turkey); (b) a short-duration event from the Sea of Marmara; (c) a short-duration event from offshore Chile. Time is given in seconds, with respect to the reference date on top of each spectrogram (yyyy-mm-dd hh:mm:ss). All examples are from the vertical component of the geophones.

et al., 2019 and references hereafter), SDEs can mostly be described by all of these characteristics: (i) short duration (<1 s), (ii) a high-frequency content (usually in the 4- to 30-Hz frequency range), (iii) amplitudes well above the noise level, and (iv) a single impulsive wave train, that is, no *P* and *S* arrivals (Figure 1). Moreover, they are recorded on one OBS at a time, suggesting a local source in the vicinity of the instrument. SDEs were first reported as fish bumps (Buskirk et al., 1981) since they were recorded on shallow instruments only and their temporal distribution showed a 24 hr periodicity. Ostrovsky (1989) then interpreted SDEs as mechanical noise produced when the instrument settles on the soft sediments bottom. In that case, large-amplitude SDEs were mostly recorded at the beginning of the experiment and unexpectedly triggered the OBS recording. Since then, SDEs have been broadly observed during many OBS experiments, yet poorly understood, although several source mechanisms have been proposed.

Sohn et al. (1995) recorded thousands of SDEs, described as microearthquakes, on the Cleft segment of the Juan de Fuca Ridge. The signals, occurring as long-lasting swarms, were associated with pressure transients in the hydrothermal system and hydraulic fracturing. A similar hypothesis was proposed in the Galicia Margin (Diaz et al., 2007), where numerous SDEs and swarms of SDEs were explained by transient and sustained pressure fluctuations, following the fluid-filled crack model usually applied to volcanic long-period events and tremors (Chouet, 1988; Chouet, 1996). More recently, Bowman and Wilcock (2014) recorded thousands of SDEs in the caldera of the Deception Island volcano, Antarctica. Although the average rate of SDEs was in good agreement with the presence of active hydrothermal vents, a diurnal pattern in the temporal distribution of SDEs lead the authors to consider two possible sources: hydrothermal activity from the seafloor and biological activity (e.g., fish bumps). In the absence of hydrophones nor video recordings, these two source mechanisms could not be distinguished.

Alternatively, Pontoise and Hello (2002) interpreted a sustained rate of monochromatic (6–7 Hz) SDEs as oscillating clouds of methane bubbles in the water column in the northern Ecuador subduction zone. From the frequency content and the number of events, they estimated the size and number of the bubbles and proposed that networks of OBS could help constrain the methane flux escaping from large areas of the seafloor. Several recent studies then suggested that SDEs originate from gas-related processes, although a correlation with the gas flux has never been established. Off southwest Taiwan, SDEs were observed together with long-lasting tremors, and based on similar frequency content (7–40 Hz) and polarization properties, both types of signals were associated to the same source mechanism (Hsu et al., 2013). Tremors and SDEs were then associated with gas emissions out of the seabed, as they both occur during the same tidal phase and with comparable amplitudes. On the other hand, long-lasting tremors were also attributed to bottom currents induced by internal tides off southeast Taiwan (Chang et al., 2016). Similarly, in the Canary

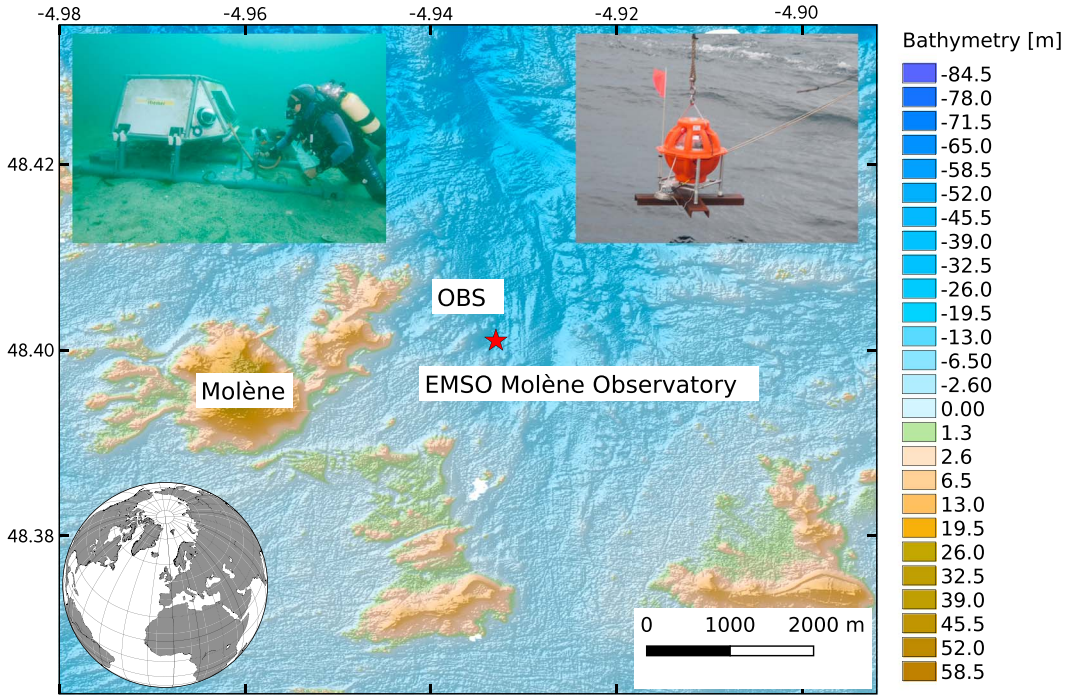

Figure 2. Seafloor bathymetry of western Brittany (Le Gall et al., 2014). The position of the EMSO-Molène observatory and the OBS is marked by a red star; insets show the localization of the study region and images of the EMSO-Molène observatory during a biannual maintenance visit and a LotOBS during deployment. EMSO = European Multidisciplinary Seafloor and water column Observatory. OBS = ocean-bottom seismometer.

Channel, harmonic tremors and SDEs were preferentially explained by environmental factors, such as sea life or transporting currents (Ugalde et al., 2019). In the Niger Delta, peaks in the number of SDEs were followed by an increase in the pore pressure and thus associated with the release of gas that accumulated in excess in the subsurface sediments (Sultan et al., 2011). In the Sea of Marmara (SoM; Turkey), multidisciplinary studies related SDEs to acoustic gas flares [Bayrakci et al., 2014], peaks in the methane concentration (Embriaco et al., 2014), conduits collapse as gas migrate (Tary et al., 2012), or conduits opening in the sediments triggered by locally large earthquakes (Tsang-Hin-Sun et al., 2019). Finally, many SDEs were associated with gas migration and seepage on the Svalbard Margin, as they occur near cold seeps and together with bottom temperature anomalies and could be easily distinguished from whale calls (Franek et al., 2017).

Considering the diversity of noise sources in the ocean, the processes involved in the generation of a SDE are numerous and possibly interacting with one another. Thus, the main limit in the analysis of SDEs is the reliable discrimination between the different sources. Due to the large number of SDEs, classification techniques, for example, using cross correlation, are hardly suitable and the use of simple discriminant parameters must be preferred. On the basis of previous studies, several questions still remain unanswered:

1. Is it possible to distinguish biological from nonbiological sources?
2. Is the source of SDEs located in the water column or in the soft sediments?
3. Are SDEs related to fluid/seafloor interactions?

In an attempt to address these issues, this paper presents observations from laboratory and in situ experiments. All data analyzed in this study were acquired by marine seismometers developed by Ifremer, called LotOBS or MicrOBS, consisting of three short-period (4.5 Hz) components of a three-channel geophone and a hydrophone, with sample frequency between 125 and 1000 Hz and a battery life of 3 weeks (MicrOBS; (Auffret et al., 2004)) to 4 months (LotOBS). While the geophones are hosted together with the acquisition system, batteries, and electrical components inside a glass sphere for the MicrOBS, geophones are deployed directly on the seafloor, outside the acquisition system for the LotOBS (Figure 2). Otherwise, both types of OBS are identical in their design. During the first experiment, two OBSs were deployed and continuously monitored by video recording for two months, taking advantage of the European Multidisciplinary

Seafloor and water column Observatory (EMSO) station north of Molène island (Brest, France; Figure 2). This unique facility permitted the direct comparison between macroscopic sources (e.g., marine fauna) near the seafloor and the seismic recordings in a coastal environment. In the laboratory, a second experiment consisted in reproducing and recording SDEs in a tank filled by sand and water to constrain the location of the source, either in the sediments or in the water column. Then, in order to investigate the deeper and more realistic oceanic conditions, SDEs were extracted and analyzed for two networks of OBS, in the SoM (Figure 3), where SDEs were mainly associated with gas emission (Embriaco et al., 2014; Tary et al., 2012; Tsang-Hin-Sun et al., 2019) and offshore Central Chile (Figure 4), where little is known about SDEs.

1.2. Geological Context of the OBS Network Regions

The SoM represents the submerged section of the North Anatolian Fault Zone, a 1,500-km-long dextral strike-slip fault separating the Eurasian and Anatolian plates (Figure 3). During the twentieth century a unique sequence of $M > 7$ earthquakes propagated westward along the North Anatolian Fault but the SoM section is the only part of the fault that has not been activated since 1766 (Stein et al., 1997) and thus poses a significant seismic hazard in the years to come. Meanwhile, the geometry of the fault system is closely related to gas-related processes as multiple hydrocarbon sources, mainly thermogenic and biogenic methane (Bourry et al., 2009; Ruffine et al., 2012), lie at shallow depth (1–6 km; Géli et al., 2018). Widespread emissions of gas from the seafloor seem to be controlled by a combination of factors such as the tectonic regime, the sedimentary cover, and the connections with the gas source (e.g., Géli et al., 2008; Dupré et al., 2015; Kuşçu et al., 2005). Acoustic techniques and submersible dives demonstrated that most of these gas emissions occur near the surface expression of known active faults [Bayrakci et al., 2014; Dupré et al., 2015], supporting a correlation between microseismicity and gas emissions (Dupré et al., 2015; Géli et al., 2018; Tsang-Hin-Sun et al., 2019).

Offshore Central Chile, the Nazca plate subducts beneath the South American plate at a rate of 6–7 cm/year, producing large earthquakes, like the 1960 Valdivia earthquake (*Mw* 9.5, 22 May 1960; the strongest earthquake ever recorded) and more recently the 2010 Maule earthquake (*Mw* 8.8, 27 February 2010). At the same time, gas hydrates are found along about one third of the Chilean accretionary wedge [eg. Grevemeyer & Villinger, 2001; Grevemeyer et al., 2003; Vargas-Cordero et al., 2017; Villar-Muñoz et al., 2014; Villar-Muñoz et al., 2018]. The analysis of seismic data revealed high concentrations of gas hydrates (17%) and free gas (0.6%), and a low-velocity zone was associated with free gas underneath the bottom-simulating reflectors (BSR; (Vargas-Cordero et al., 2017)). Systematic mapping of the BSR from a reflection seismic profile near our study area suggests that the gas hydrate layer is about 290 m thick on average, which might represent a methane budget of about 3×10^{13} m^3 at standard pressure-temperature conditions (Villar-Muñoz et al., 2014; Figure 4). The authors concluded that a sudden or slow release of this amount of methane, in the event of gas hydrate dissociation, might represent a sizable geological hazard, destabilizing marine sediments and potentially triggering earthquakes and tsunami waves.

This study aims at characterizing the nature of the SDEs in different marine environments and at understanding their relationship with the seafloor and water column processes (e.g., seismic activity, biological activity, tides and currents, and fluid-related processes).

2. Data Acquisition and Processing

2.1. Description of the OBS Experiments

All data analyzed in this study were acquired by marine seismometers developed by Ifremer. Technical details on each experiment are given in Table S1 in the supporting information.

2.1.1. Marmara Data Set

A submarine network of 10 OBSs was deployed by Ifremer from 15 April to 31 July 2011 in the western SoM (Figure 3) in order to study and better characterize the microseismicity in an area where gas is likely present in the upper sediment layers (Figure 3). The instruments consisted of LotOBS, recording at a rate of 8 ms (125 Hz). The central station of the network, OBS02, did not function properly and stopped recording on 30 June 2011. Note that OBS03 was excluded from the analysis since the recordings were corrupted by a periodic glitch producing an impulse signal quite similar to SDEs.

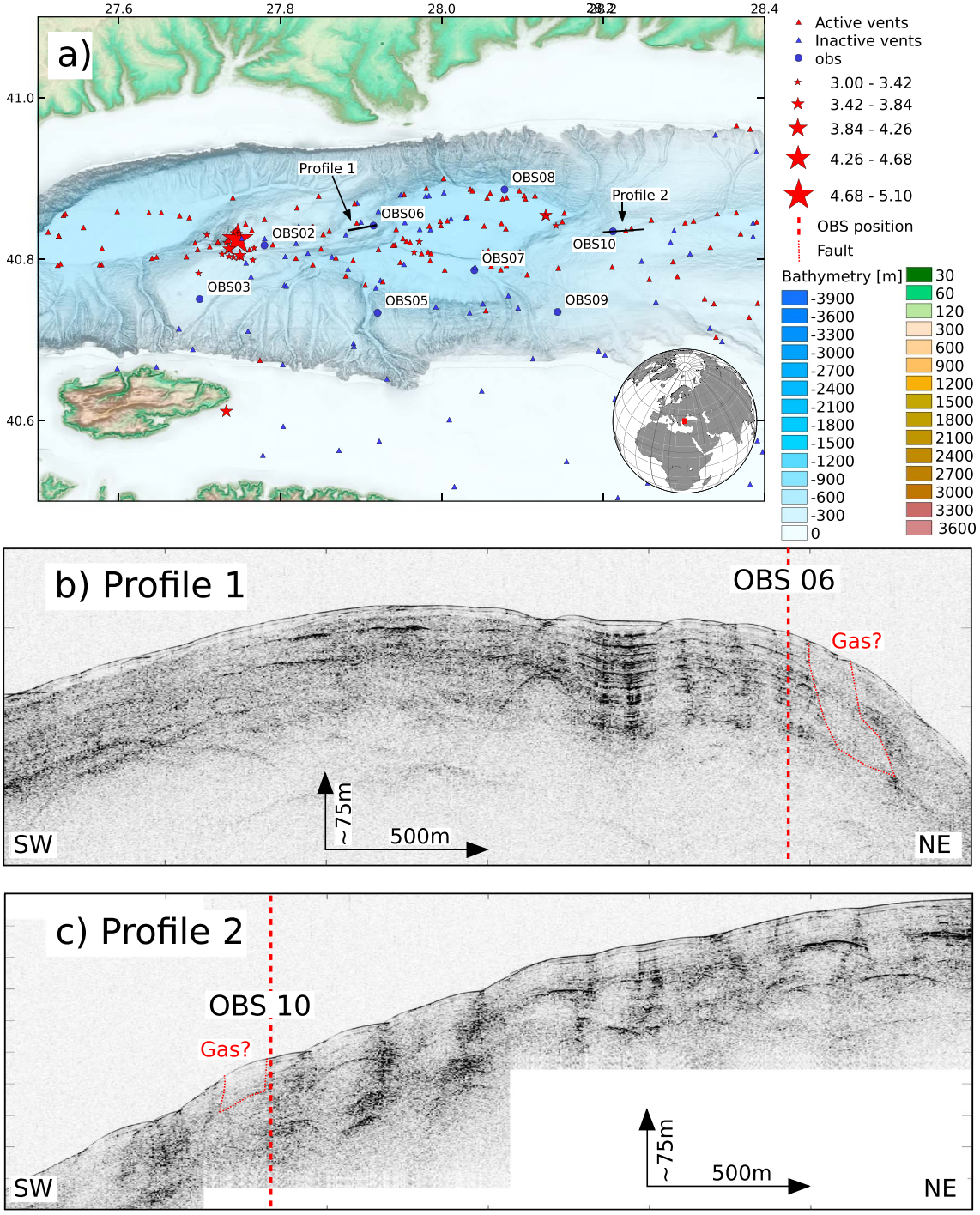

Figure 3. (a) Bathymetry of the Sea of Marmara with the location of the OBS stations marked as blue circles. Active vents are marked by red triangles and earthquakes by red stars with their size scaled to the magnitude and location of profiles in (b) and (c) are marked by black lines. (b) Sediment penetrator profiles (chirp source ~3.5 kHz) near OBS6. Blanked areas indicated by dotted red lines suggest the likely presence of gas in the upper sediment layers near OBS6 site, which position along the profile is indicated with thick vertical dashed red lines. (c) Same as (b) but for OBS10 site. OBS = ocean-bottom seismometer.

2.1.2. Chile Data Set

A temporary offshore seismic network of 17 OBSs was installed after the 2010 Maule earthquake (*Mw*8.8; 27 February 2010) off Central Chile, in order to better constrain the geometry of the rupture zone and its lateral extent (Figure 4). The instruments were micrOBS from the National Taiwan Ocean University and the Central Taiwan University, deployed within the central portion of the rupture zone from roughly 36°S to

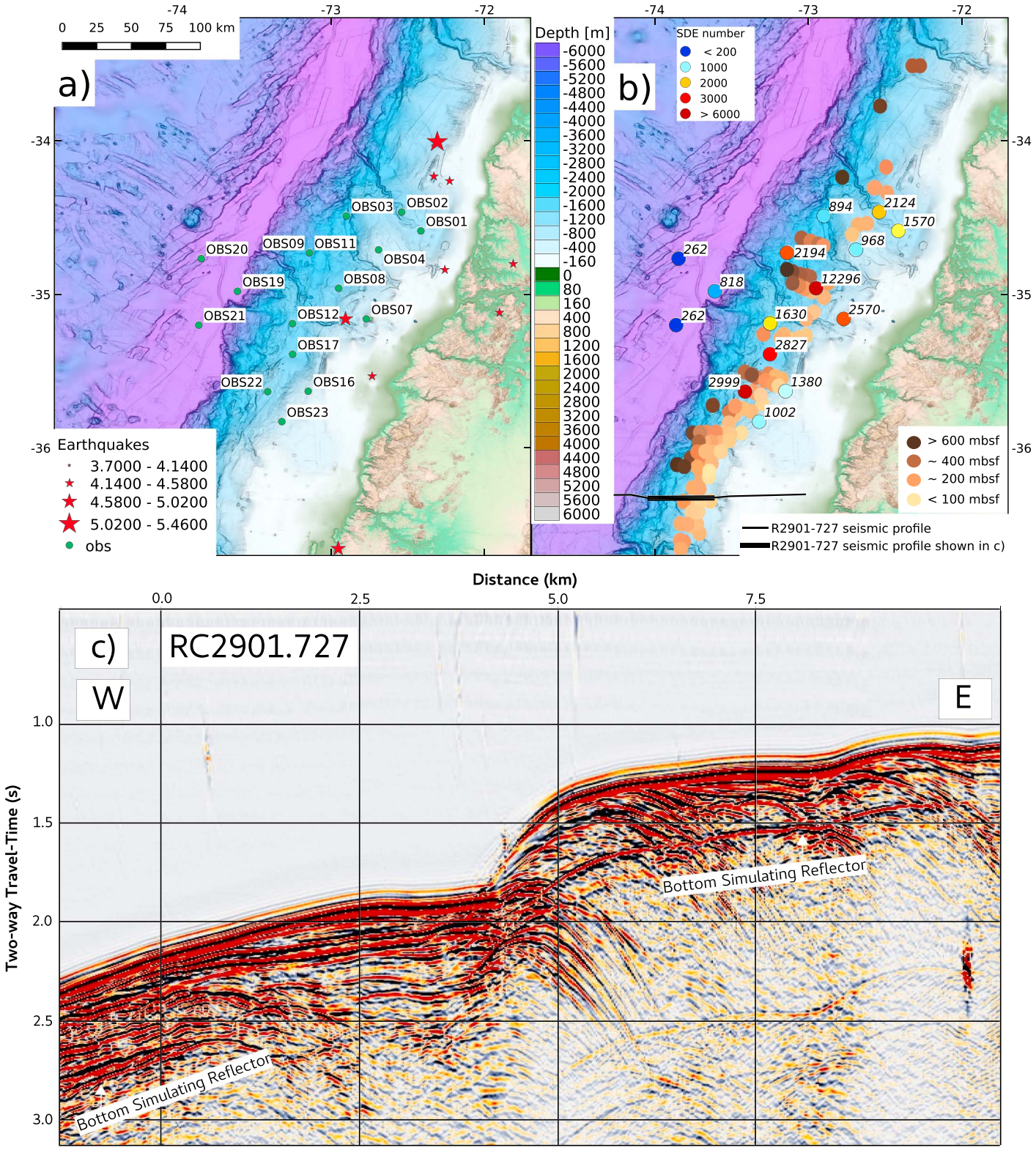

Figure 4. (a) Bathymetry offshore Central Chile [Ryan et al., 2009] and the location of the OBSs (blue circles) and earthquakes (red stars with sizes dependent of the magnitude). (b) Comparison between the number of short-duration events recorded at each OBS and the location of the bottom-simulating reflectors [from Villar-Muñoz et al., 2014]. The number of short-duration events recorded at each site is indicated as annotations and rainbow colors; light to dark brown circles without annotations are the bottom-simulating reflectors depth [from Villar-Muñoz et al., 2014]. The seismic profile of (c) is marked by a black line with the bold part corresponding to the extent of the seismic data shown in (c). (c) Bottom simulating reflector along the profile RC2901.727. OBS = ocean-bottom seismometer.

34.5°S and recorded earthquakes during three weeks in July–August 2010 (Figure 4). Out of the 17 OBSs, 2 did not function properly and were thus excluded from the analysis.

2.2. Detection of the SDEs

For every in situ data sets, SDEs were automatically detected by applying a recursive short-term average/long-term average algorithm, provided by the Python-based ObsPy toolbox (Beyreuther et al., 2010) to the whole detrended, unfiltered time series. The processing was applied to all vertical components, but similar results were obtained for the horizontal components. However, as horizontal components are highly sensitive to the horizontal orientation of the instrument, we chose to use the vertical components only for our analysis. Adequate detection parameters, such as the length of the short and long windows (0.35 and 7 s, respectively), trigger/detrigger threshold levels (8/2) and time buffer added before the trigger time (0.075 s) were selected after a careful analysis of different sets of values and tested on a randomly chosen 1-hr data sample; triggers from automatic detection were then visually checked and compared to the manually picked events (Figure S3). To further discriminate SDEs from earthquakes, only triggers lasting less than 1.1 s were considered. The optimal parameters are those giving the maximum number of SDEs at the same time as none false trigger, earthquake, or electronic noise.

2.3. Source Characterization

SDEs are usually not recorded on several instruments at a time. Therefore, classical location techniques are not applicable. As the signals are recorded on three-component sensors, it is possible to determine the direction of the source, by computing the back azimuth, that is, the angle between the station and the source. The back azimuth is estimated from the particle motion in the horizontal plane (Figure S3). Prior to the back azimuth estimation, the misorientation of the horizontal components of the OBS deployed in the SoM was determined as in Tsang-Hin-Sun et al. (2019), using the technique of Niu and Li (2011). The horizontal components of the OBS deployed in Chile are not oriented with respect to the geographic north, so the estimated back azimuth does not represent the true direction of the source. Since the experiment lasted only 3 weeks, it was not possible to determine the OBS misorientation. Nonetheless, this uncertainty does not affect the possible temporal trends in the back azimuth.

Additionally, the dominant frequency of each SDE was extracted from the 256-point spectrum for each individual event. The dominant frequency is the one carrying the most energy in the spectrum and is usually a good proxy for source identification in the oceanic soundscape (Figure S3). An individual SDE can finally be described by three source parameters: the arrival time, the dominant frequency, and the relative/real back azimuth for misoriented/oriented components.

3. Field and Laboratory Experiments

3.1. Test 1: Can the Interaction of the Marine Fauna and the OBS Produce a SDE?

The EMSO-Molène station is a multidisciplinary cabled observatory operated by Ifremer since June 2012, in the scope of the EMSO project, and serves as a pilot for industrial applications of surveillance in marine regions. The platform, composed of several connected instruments, including a video camera, is sheltered by currents and swells by a rocky frame. The water depth at the EMSO-Molène observatory ranges from 12 to 18 m and is thus in the photic zone. Two LotOBS from Ifremer were installed in the field of vision of the observatory between 27 April and 13 June 2016, separated by ~1 m. Images of a resolution of 1,280 × 720 pixels were taken every 2–3 s during the daylight hours.

The Molène archipelago, offshore Brittany (Figure 2), is located in a marine protected area hosting a large seaweed field, a wide range of benthic organisms and marine mammals like bottlenose dolphins and seals. Tides are important, up to 8 m, and strong currents fashioned submarine canyons as revealed by the high-resolution bathymetric data available in the region (Klingelhoefer et al., 2017; MeDON survey, 2011; Figure 2).

The visual inspection of the snapshots reveals an active fauna in the vicinity of the observatory, including several species of fish, mollusks, and crustaceans. However, direct interactions between the animals and the instruments rarely occurred, even when their presence was dense and the recorded signals on the geophones were easily distinguishable from a typical SDE. For example, a spider crab moving on the

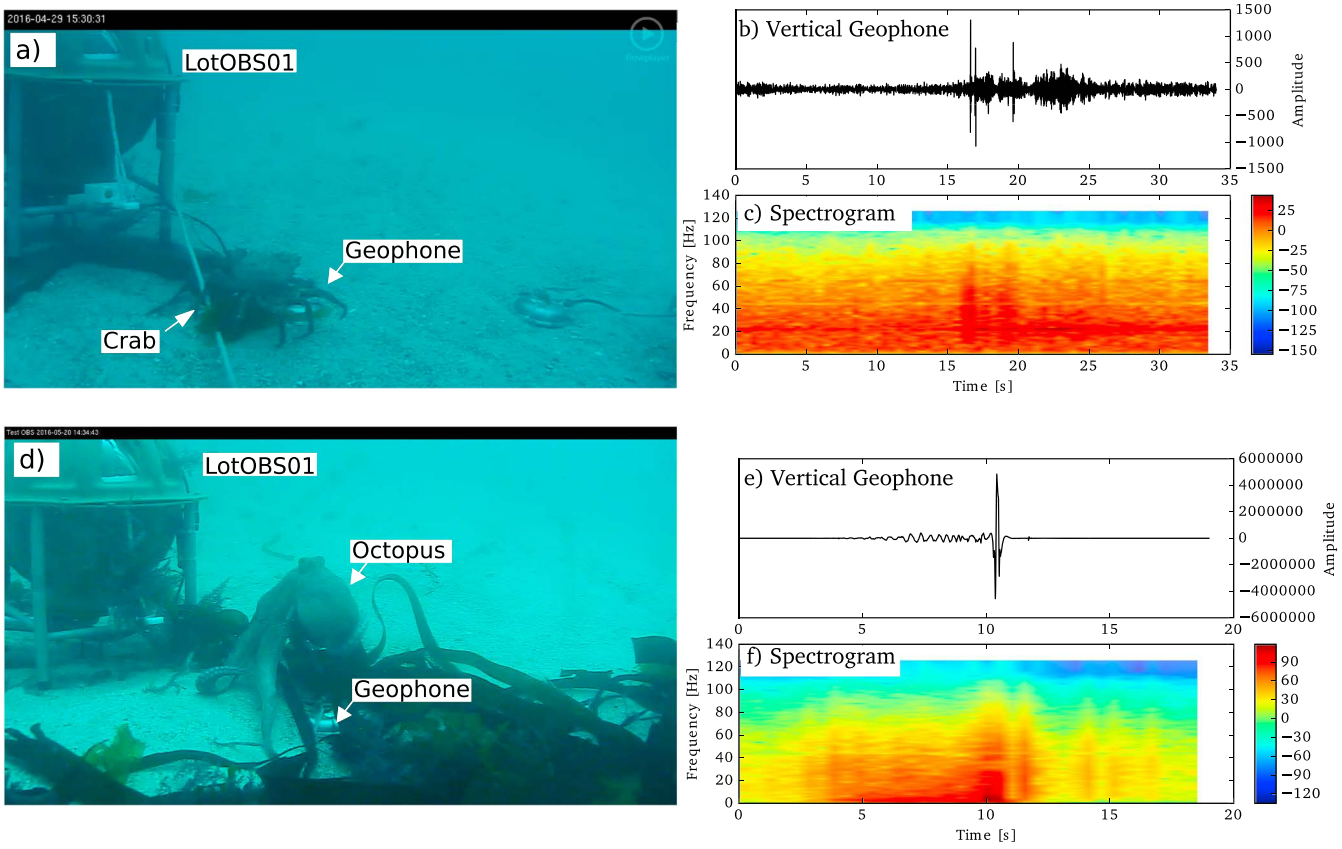

Figure 5. Top panels: Image of a crab moving around the geophone of LotOBS01 (a), associated waveform (b), and spectogram (c). Bottom panels: image of an octopus on the geophone of LotOBS01 (d), associated waveform (e), and spectrogram (f).

geophone, produced a long (>10 s) wave train in the 40- to 60-Hz range (Figures 5a and 5b); an octopus created some low-amplitude noise as the animal is approaching and a high amplitude but irregular event (1–2 s), while the animal is crossing over the geophone (Figures 5c and 5d). It is worth noting that the maximum amplitude during the crossing is 6×10^6V/m/s, which is a similar value as a typical earthquake of magnitude 3–4 some tens of kilometers from the instrument.

Bottom currents and back-washing waters are clearly visible during the whole experiment, transporting sand and plant particles. Indeed, a large number of seaweed strands flowed in the vicinity of the OBS, sometimes without any interaction but often brushing against them. Fragments of seaweed sometimes got trapped in the cables or in the OBS frame, yielding long-lasting tremor-like signals on the seismograms. From time to time, a fragment of seaweed hit a single OBS and produced a short impulsive signal on the geophones, but this rarely occurred. The temporal distribution of SDEs shows a clear 24-hr periodicity and a possible second-order 12-hr periodicity (Figures 6a and 6d), suggesting that tidal currents are involved in the generation of SDEs. From the end of May 2016, the number of SDEs falls on both OBSs. At the same time, the video recordings show that seaweeds have progressively accumulated on and around the instruments. In June, the video recordings were no longer usable since the instruments were completely covered with seaweed. The dominant frequencies span a broad range, from 50 to 90 Hz, 50% of the time and a median value around 75 Hz (Figure 6e). Outliers, however, are distributed over the whole spectrum, suggesting random source of noise. The back azimuth analysis shows that most of the SDEs originate from a preferential direction that does not change much during the experiment (between 60° and 90°; Figure 6b). All of these observations suggest that SDEs are mainly related to transporting currents, with a dominant 24-hr periodicity, and that the accumulated seaweeds then acted like a shield from the end of May 2016. The geological setting (e.g., coarse, shell sand covering Paleozoic rock) excludes gas seepages as the source of the Molene's SDEs.

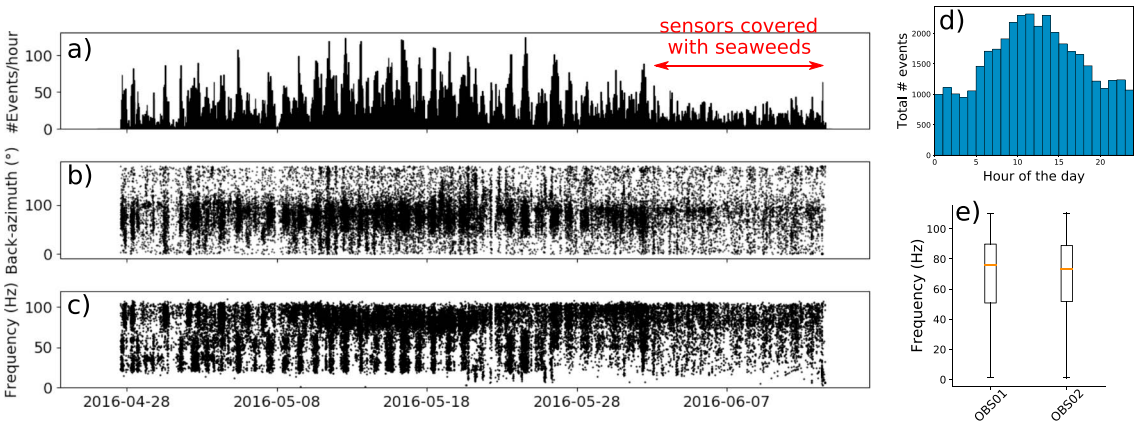

Figure 6. Source parameters of the short-duration events (SDEs) recorded near the Molène island. (a) Temporal distribution of the hourly rate of SDEs; (b) temporal distribution of the associated back azimuths; (c) dominant frequencies for OBS01; (d) distribution of the SDEs according to the hour of the day; and (e) the statistic distribution of the dominant frequency of SDEs for OBS01 and OBS02. The thick orange line represent the median frequency, and the box contains 50% of the distribution. The whiskers are the 10th and 90th percentiles of the distribution.

3.2. Test 2: Can a SDE Be Reproduced in a Laboratory Experiment?

The second experiment was conducted in the laboratory in order to verify that SDEs could be linked to fluid-related processes, as proposed by many authors in different contexts (SoM, Tary et al., 2012; Tsang-Hin-Sun et al., 2019; Taiwan, Hsu et al., 2013; Svalbard Shelf, Franek et al., 2017; Galicia Margin, Diaz et al., 2007; and Antarctica, Bowman & Wilcock, 2014) and to compare the location of the source in the water column or in the sediments. The experimental setup is composed of an OBS deployed in a tank filled by 12 cm of sand superimposed with 20 cm of water (Figure 7). Next to the OBS, an air supply regulated by a pressure gauge was installed, so a fluid could be injected in the sand layer or in the water column. Three series of tests were performed:

3.2.1. Case 1: Injection of Air Within the Sand Layer

The first series of tests consisted in injecting air in the sediments, so it can eventually reach the surface. Before the air bubble leaves the sand layer, an updoming of the surface can be observed, which then bursts as the volume of air increases. We also observed that an air bubble tends to follow the path of earlier ones, as previously proposed by Algar et al. (2011a) based on numerical modeling. On the geophones, each bubble

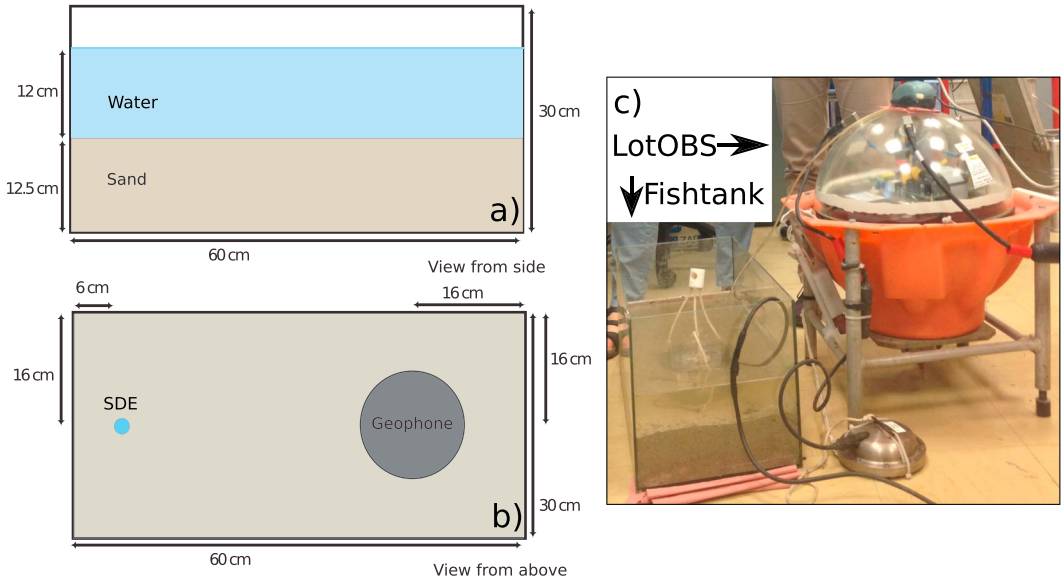

Figure 7. Experimental setup for the laboratory experiment from side (a) and top view (b) and (c) photography of the setup.

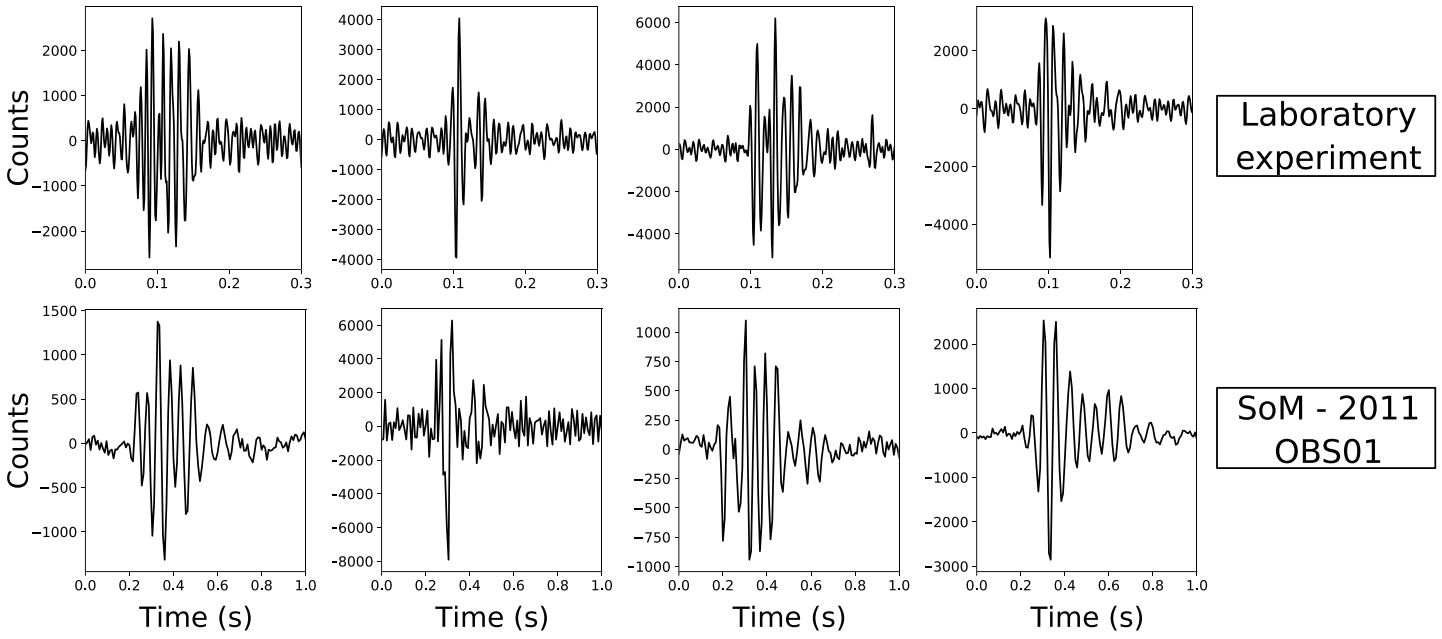

Figure 8. Comparison between short-duration events obtained during the Case 1 of the laboratory experiments and short-duration events recorded in the Sea of Marmara on OBS01. All plots show the vertical component. The signal from the laboratory experiment was band-pass filtered in the 70- to 200-Hz range. The time scale is different for both data sets, reflecting the differences in the frequency content.

injected in the sand layer produces a signal of short duration (<1 s). Because the experiment was conducted in the laboratory, the conditions and scales are drastically different from those of the real OBS deployments. A high level of persistent noise contaminates the OBS recordings at a frequency ~50 Hz (due to the power supply) and below (due to urban noise), making a frequency analysis of the signal difficult. After filtering the time series in the 70- to 200-Hz frequency range, the waveforms of the SDEs appear with a satisfying signal to noise ratio (Figure 8).

3.2.2. Case 2: Injection of Water in the Sand Layer

Releasing water into the sand layer does create very similar results. As a matter of fact, in these experiments it is not possible to discriminate between gas and fluid expulsions from the sand layer.

3.2.3. Case 3: Injection of Air in the Water Layer

Tests consisting in releasing the gas directly into water resulted in no or only very weak signals on the geophones and therefore suggest that SDEs are not likely to be generated by the acoustic resonance or fluid bubbles in the water column.

Although not fully quantitative, these simple experiments suggest that gas-related processes, such as gas or fluid seepage out of soft sediments, might produce nonseismic signals similar to SDEs (Figure 8). In our analog experiments, the frequency of the signal is much higher than for real SDEs and thus not directly comparable. Nonetheless, there is a similar diversity of waveforms (e.g., sharp or emergent onset, lower-frequency coda, and very short or longer events). It is expected that at much smaller scale (here the fish tank), smaller wavelengths would be at play, thus yielding higher frequencies. Moreover, the dominant frequency of vibration of the system might also be controlled by the gas pressure, the size of the fluid conduit, the nature of the sediments (density, water content, and compaction), or the depth of the source. Many other sources are, however, able to produce similar waveforms and the main difficulty lies in their discrimination in real data sets.

4. SDE Analysis in the SoM

4.1. Previous Observations

In the SoM, the occurrence of numerous SDEs has been widely reported (e.g., Embriaco et al., 2014; Tary et al., 2012; Tsang-Hin-Sun et al., 2019) and related to the presence of free gas in the sediments and cold seeps (Dupré et al., 2015; Géli et al., 2008). Indeed, there is a direct relationship between gas-rich structures and the

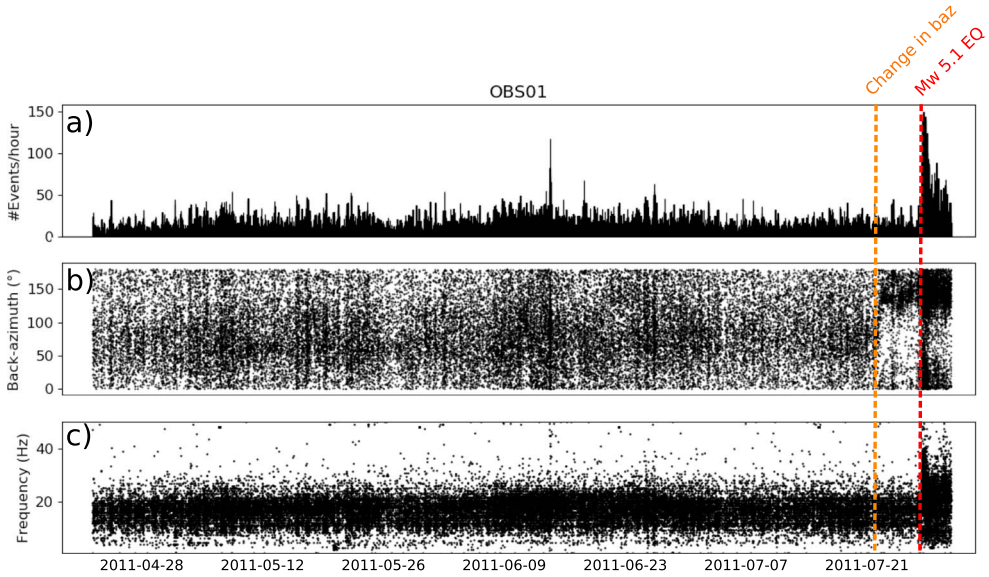

Figure 9. (a) Temporal distribution of the hourly rate of short-duration events; (b) temporal distribution of the associated back azimuths and (c) dominant frequencies for OBS01 in the Sea of Marmara. The first vertical dotted line marks a clear change in the orientation of individual short-duration events, while the second dotted line mark the occurrence of the *Mw* 5.1 earthquake that triggered gas emission. Adapted from Tsang-Hin-Sun et al. (2019).

distribution of SDEs. For instance, in 2011, OBS04 and OBS01 detected the highest number of events and are located on the top of the Central High, a gas-rich anticline and near a buried mud volcano, respectively (Figure 3; see also Bayrakci et al., 2014, and Tsang-Hin-Sun et al., 2019, for a complete review). On the contrary, areas with a low to moderate SDEs activity match the regions where no or little gas was reported.

On 25 July 2011, a *Mw* 5.1 earthquake occurred just 10 km southeast of OBS01, triggering a long-lasting tremor and a large crisis of SDEs, lasting several days, interpreted as fracturing in the sediments and consecutive gas migration in the opened conduit near OBS01 (Tsang-Hin-Sun et al., 2019). Interestingly, few days before the mainshock, the back azimuth of the SDEs spontaneously changed from randomly scattered orientations to ~N150° (or N300°), in the direction of the epicenter (or the opposite direction due to the 180° ambiguity; Figure 9). The SDEs then originated from the same direction, suggesting a common source location. However, aside from this spatial reorganization, neither the temporal variations in the rate of SDEs nor the dominant frequency of the events departed from the previous trend, suggesting a common source mechanism, that is, related to gas, for all the events. Within this study we aim at better characterizing these gas-related SDEs depending on their source parameters defined as their temporal mode of occurrence, their spatial distribution (back azimuth), and their dominant frequency.

4.2. Source Parameters of Gas-Related SDEs

Gas-related SDEs in the SoM can be classified into two families, based on their temporal mode of occurrence and their spatial clustering: background and swarmed SDEs.

4.2.1. Background SDEs

In most cases the SDEs occur individually, at a rate of a few tens of SDEs per hour, on a nonregular basis. Their amplitudes are highly variable, and they are scattered in all directions. Background SDEs are observed over the whole network and not correlated between stations. They are also observed in areas where no gas activity has been reported, suggesting unrelated and local sources. The dominant frequency of background SDEs ranges from 4 to 30 Hz but mostly focus in the 14- to 18-Hz range.

4.2.2. Swarmed SDEs

From time to time, SDEs cluster in both time and space as sequences of hundreds of events per hour, lasting up to several hours and even several days (Figure 10). Swarmed SDEs originate from preferential directions that can be recurrently activated in time (e.g., Tsang-Hin-Sun et al., 2019). The dominant frequency of swarmed SDEs is generally within the same range as background SDEs, although during the largest swarms it can reach higher values.

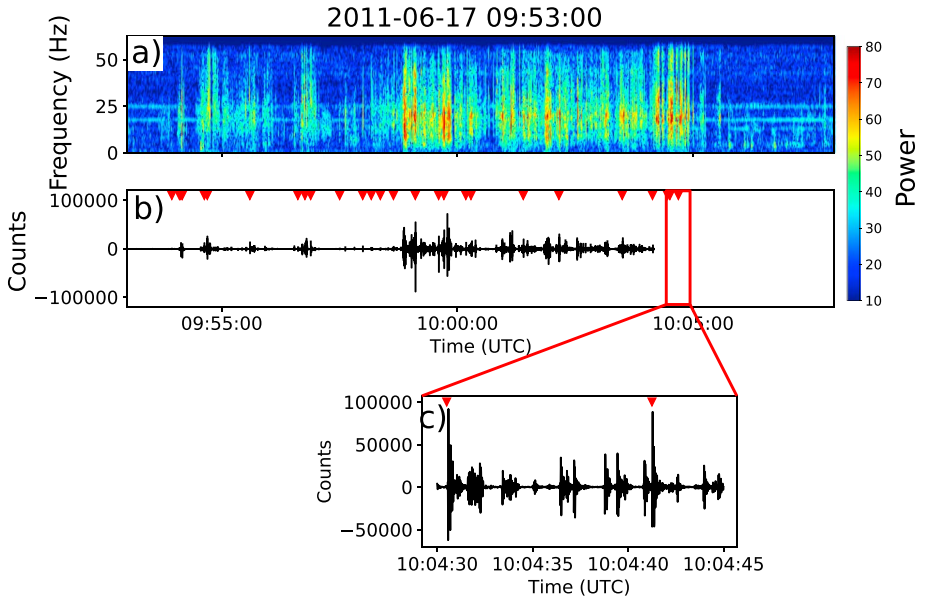

Figure 10. Example of a swarm of short-duration events recorded on the vertical component of OBS01 in the Sea of Marmara. (a) Normalized spectrogram, computed for 128-sample segments and 50% overlap, representing the distribution of the power in time and frequency; (b) seismogram of the vertical component, detrended, unfiltered; the detected short-duration events are indicated by red triangles. (c) A close-up of the data samples included in the red box. Time is given in hh:mm:ss, and the initial time is given above the top panel.

Across the whole study area, the distributions of background and swarmed SDEs are very similar. More specifically, the distribution of the dominant frequency is remarkably steady, with median values in the 14- to 17-Hz range (Figure 11). Moreover, 50% of the time, frequencies range from 12–15 to 21–22 Hz, gathering in a narrow band around the median values, whereas extreme values reach 4 to 30 Hz. We note that this similarity in the frequency distribution does not depend on the depth, nor the event rate. The experiments [this manuscript] conducted by Ifremer in the lab and at sea revealed that SDEs could be produced by any kind of small perturbation affecting the seafloor sediments (e.g., sediment motion driven by bottom currents and fluid transfer at the sea bottom). The uniformity in the frequency clearly suggests similar sources, even a unique type of source, all over the SoM, consistent with a gas-related origin.

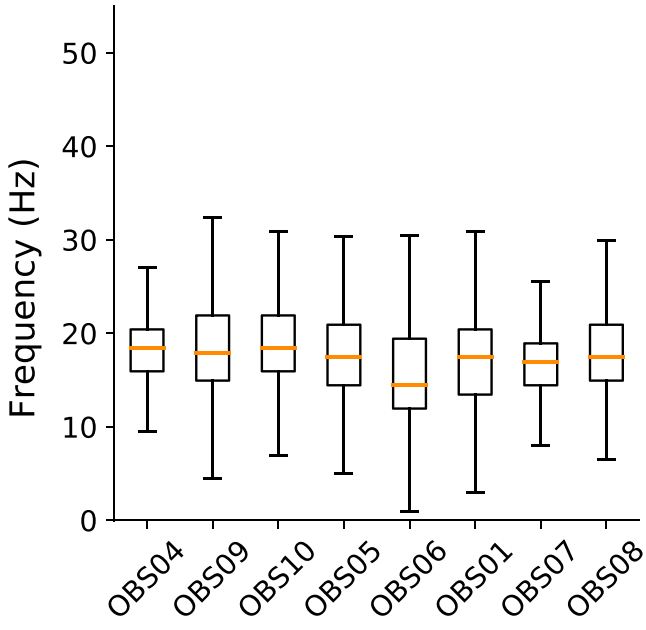

Figure 11. Distribution of the dominant frequency of short-duration events at each ocean-bottom seismometer in the Sea of Marmara. The distributions are represented as boxplots; the thicker orange line is the median value, the box contains 50% of the distribution (between the 25th and the 75th percentiles), and whiskers represent the 10th and 90th percentiles. The ocean-bottom seismometers are sorted according to increasing depth.

Since both background and swarmed SDEs have similar waveforms, amplitude, dominant frequency, and eventually back azimuth (Figures 9 and 10), they are most probably generated by the same source mechanism: By analogy with volcano-tectonics events (e.g., Chouet, 1988) or hydrothermal events (e.g., Diaz et al., 2007), background SDEs are proposed to be generated by transient pressure perturbations in the fluid-filled cracks, whereas swarmed SDEs reflect a sustained excitation of the medium, for example, due to fluid migration within the cracks.

5. SDE Analysis Offshore Central Chile

5.1. Observations

In comparison to the SoM, the average daily rate of SDE is moderate over the Chilean study area. There is no linear relationship between water depth and the number of SDEs recorded. Instead, the number of SDEs is generally higher at very shallow (>500 m) and intermediate depth (~1,500–3,000 m) and lowest at the deepest sites (>4,000 m). OBS08

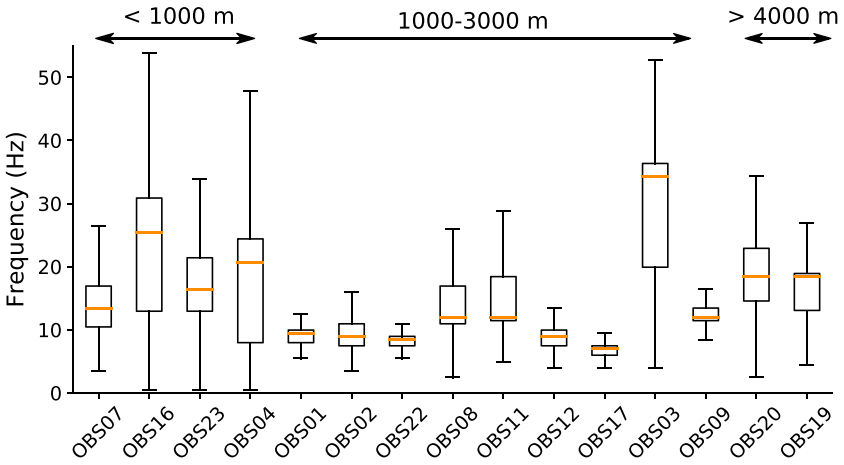

Figure 12. Same as Figure 11 for the ocean-bottom seismometers offshore Chile. The depth range of the ocean-bottom seismometers is indicated on top.

appears as an outlier, recording 3 times more events than the neighbor OBSs at intermediate depth. This regional trend is enhanced when considering the distribution of the dominant frequencies of the events (Figure 12). Shallow (<1,000 m) and deep (>2,500 m) sites have a median dominant frequency above 12 Hz, with outliers reaching 50 Hz and a broad range of frequencies, possibly indicating multiple sources. On the contrary, at intermediate depth, the distributions gather around a low median value (≤12 Hz). We note that this trend does not depend on the number of events and is thus not a bias from the detection method.

The joint analysis of the temporal variations in the event rate, back azimuth and dominant frequency, might point to the source discrimination for shallow, intermediate, and deep sites. At the shallow OBS16, for instance (Figure 13), SDEs occurred regularly in time and are generally scattered in all directions, except at the end of the experiment where they cluster in time and space (around 40°). The dominant frequency does not vary in time, although it falls into two distinct frequency ranges, around 12 Hz and in the 22- to 35-Hz range, respectively.

At the intermediate depth site OBS12, SDEs occur irregularly in time and are generally scattered in all directions. The dominant frequencies are mostly clustered in the 8- to 13-Hz frequency band, with some exceptions. There are several peaks in the temporal rate of SDEs that can also be clearly identified in the temporal distribution of back azimuth and dominant frequency. The first peak is clustered in frequency around 20 Hz and shows a fast change in the temporal variation of the back azimuth, indicating a moving source. This spatiotemporal pattern is repeated several times during the experiment and was observed at different sites, from intermediate to deep sites, indicating a moving source of SDEs. The visual inspection of such features indicate pulse series of short signals (~1 s) with a dominant frequency around 20 Hz. On the other hand, the second peak, although similar in the number of events, exhibits a nonlinear spatiotemporal pattern and has dominant frequencies in the same range as the background SDEs (Figure 13). The visual inspection of the data revealed a signal very similar to the tremors or swarmed SDEs previously identified in the SoM.

Finally, at the deep OBS19, SDEs occurred regularly with a low rate, except for the two large peaks on 20 and 30 July 2010. As observed on OBS12, the events have a constant dominant frequency in the 18- to 25-Hz range and exhibit linear spatiotemporal features. Otherwise, the rare SDEs are scattered in all directions and have dominant frequencies in the 4- to 25-Hz frequency range.

5.2. Possible Sources of SDEs in Chile

5.2.1. Biological Activity

Short-duration signals with similar features than our pulse series, that is, frequency around 20 Hz and moving source, were observed by Franek et al. (2017) and attributed to fin whales offshore Svalbard. In the Southeast Pacific, blue and fin whales are known to produce acoustic signals in the same frequency range

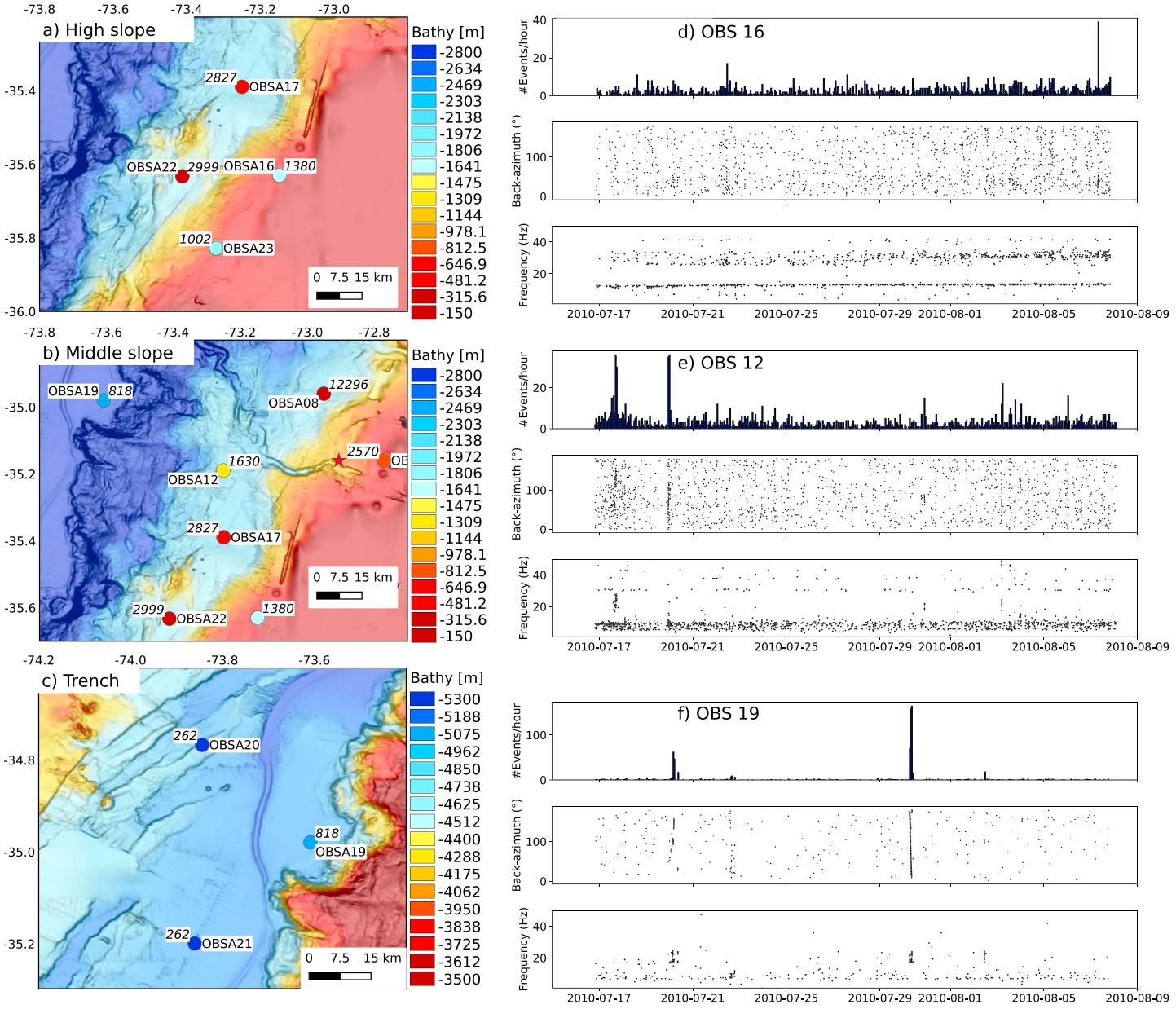

Figure 13. Bathymetry and source parameters of SDEs for shallow (a, d), intermediate (b, e), and deep conditions (c, f). (a) Bathymetry around OBS 16 on the high slope; (b) bathymetry around OBS 12 on the middle slope; (c) bathymetry of OBS 19 in the deep sea. (d) Number of events per hour (upper subpanel), back azimuth of SDE (middle subpanel), and frequency of SDE (lower subpanel) for OBS 16; (e) as (d) but for OBS 12 and (f) as (d) but for OBS 19. On the bathymetry maps (a)–(c), the number of SDEs recorded at each OBS is indicated and represented with the same color scale as in Figure 4. OBS = ocean-bottom seismometer; SDE = short-duration event.

[e.g., McDonald et al., 1995]. Chilean blue whales, however, have longer characteristic call units (37 s; McDonald et al., 2006) and a repeating pattern that does not match the observed pulse series. Fin whales are observed all year-round in the North and South Pacific [McDonald et al., 1995; Soule & Wilcock, 2013] and offshore South Chile (Acevedo et al., 2012). Fin whales typically produce characteristic and short calls termed "20-Hz pulses" (Watkins, 1981), similar to the observed pulse series. We thus propose that the pulse series observed at intermediate and deep sites are produced by fin whales. During the three weeks of the experiment, fin whales were mostly recorded to the west, far from the coast and at deep sea, which is consistent with previous observations (Acevedo et al., 2012).

SDEs due to fish bumps have a diurnal pattern of occurrence that is not observed in our data (Buskirk et al., 1981). It is also unlikely to explain the regional pattern in the distribution of SDE with marine animals interacting with the instruments. Moreover, most of the events (disregarding the identified whale calls) are not visible on the hydrophone, indicating that the source is not located in the water column. Biological sources other than marine mammals are thus not likely to be the main source of the observed SDEs.

5.2.2. Tides and Currents

Tides and currents are able to generate SDEs and tremors resembling ours by agitating the sensors in their natural frequency of oscillation (Chang et al., 2016). Local turbulent flows might also be responsible for some background SDEs, as observed in Molène or in the Canary Channel (Ugalde et al., 2019). Strong seasonal currents have been described offshore Chile, with a vertical structure depending on several factors (Shaffer et al., 1995). Currents are, however, more powerful in austral spring and summer and exhibit a diurnal periodicity, which is not retrieved in the temporal distribution of SDEs, even if the duration of the experiment is not suitable to infer a robust temporal pattern in the distribution of SDEs. Moreover, currents are expected to be stronger at shallow depth, which is not consistent with the pattern in the spatial distribution of SDEs. Nevertheless, transient and local currents, induced by bathymetric features such as canyons and corridors, might also produce noise at a smaller scale. Offshore Chile, as it was the case in the SoM, no direct relationship was established between the bathymetry and the rate of SDEs.

5.2.3. Gas-Related Activity

In the intermediate depth range (1,500–3,000 m), corresponding to the accretionary wedge of the subduction zone, the distribution of the dominant frequency points to a main unique source of SDEs. As for the SoM, background SDEs and swarms of SDEs were observed, sharing similar characteristics in term of frequency and spatiotemporal features.

Comparing the number of SDEs recorded for each instrument with the extension of the BSR along the accretionary wedge [Villar-Muñoz et al., 2014] shows a good correlation between the intermediate domain identified for SDEs and the region of the BSR (Figure 4b). We therefore propose that SDEs observed at intermediate depth, that is, having a similar dominant frequency ~12 Hz and occurring as individual events or swarms, could be related to free gas migration in the sediment layers.

6. Discussion and Conclusion

6.1. From Experiments to Real Conditions

The main objective of this study was to test different hypotheses for the origin of short-duration signals frequently recorded by OBSs, in different contexts. For that purpose, we combined laboratory and in situ observations to explore different sources and to rule out some of them.

The first test of this study consisted in continuously monitoring two OBSs using a submarine video camera and show that no fish accidentally bumped into the instruments. Although some animals, such as crabs or octopus might cross the OBSs or move nearby, the associated waveforms are substantially different from the SDE waveforms. Fish, even when numerous, are not detected by either the geophones or the hydrophone. Seaweed or lithic particles transported by the tidal currents produce, however, short-duration signals of high frequency distributed with a clear temporal periodicity. Even if the water depth at the EMSO platform is only a few meters, some of these observations can be extrapolated to the deep sea. If the various macroscopic fauna from Molène do not interact with the OBSs, it is unlikely that this would occur at deep sea. Thus, fish bumps should be ruled out as a systematic source of SDE. Many SDEs resembling ours in the SoM were recorded in the caldera of Deception Island volcano (Antarctica; Bowman & Wilcock, 2014); the authors, however, were unable to conclude whether they were caused by marine animals striking the instruments or hydrothermal activity. In the light of our observations, it is much more probable that an intense hydrothermal activity is the cause of the observed SDEs.

During the second test, qualitative analog experiments showed that SDE waveforms can be reproduced, to some extent, by expelling a fluid from a sand layer. In comparison with the real SDEs, they have a much higher-frequency content, which could be explained by smaller wavelengths, controlled by the size of the system (60 cm * 30 cm * 30 cm). Moreover, in real conditions, the dominant frequency of vibration might also be controlled by the nature of the sediments, the diameter of the conduits and the average pressure fields of gas and sediments. Expelling a fluid directly into the water column did not produce any signal

on the geophones, suggesting that the source of the observed SDEs, even more in the deep sea conditions, is located at or below the seafloor rather than in the water column. Quantitative experiments demonstrated that the initial rise of a bubble in sediments is performed by fracturing of soft and cohesive sediments (Boudreau, 2012; Boudreau et al., 2005). In our simple experiment, it was possible to infer gas exchanges by measuring the number and the size of bubbles. In more realistic conditions, the volume of a bubble depends on its shape, which can differ from an ideal sphere, and is thus conditioned by several physical factors, such as softness or cohesion of the sediments [e. g. Johnson et al., 2002]. However, assessing the amount of gas released in the water column with SDEs, although a seductive idea, is beyond the scope of the study.

In the SoM and offshore Chile, a good relationship between the location of cold seeps (Tsang-Hin-Sun et al., 2019) and BSR (this study) is found, respectively, and the distribution of SDEs, suggesting that gas-related processes generate the observed signals on the OBSs. In the SoM, SDEs have been related to free gas migration through multidisciplinary approaches, including modeling (Tary et al., 2012), acoustics [Bayrakci et al., 2014], or methane flux measurements (Embriaco et al., 2014). More recently, SDEs were directly associated with a conduit opening in the soft sediments triggered by a *Mw* 5.1 local earthquake (Tsang-Hin-Sun et al., 2019). The SDEs in the SoM are characterized by

1. two temporal modes of occurrence, individual events, and swarms of events,
2. a limited range of dominant frequency with few variations with respect to the median value, and
3. punctual temporal and spatial clustering of individual or swarmed events.

Laboratory experiments have shown that a bubble injected into sediments tends to follow the same path as previous bubbles (Algar et al., 2011b). Depending on the gas injection rate, Varas et al. (2009) also described two modes of fluid emission: a bubbling regime where large, individual bubbles are formed and an open-channel regime, where small bubbles are continuously growing. In time, a cold seep can also change from a mode of intense emission to a more quiet mode (Römer et al., 2017), under the influence of an earthquake (Tsang-Hin-Sun et al., 2019) or tides (Hsu et al., 2013; Römer et al., 2017). This temporal pattern in the mode of occurrence of SDEs was also reported offshore Taiwan (Hsu et al., 2013), in Svalbard (Franek et al., 2017), or in the Galicia Margin (Diaz et al., 2007). In all these cases, background and swarmed SDEs were associated with the same type of source, as they had similar waveforms, dominant frequencies or back azimuths. In Chile, the SDEs recorded on the accretionary wedge and associated with the BSR have comparable source parameters, suggesting that this combination of parameters is well calibrated for discriminating gas-related SDEs. The same source parameters also allowed the identification of biological signals produced by fin whales in Chile or by tidal currents in Molène.

6.2. Implications for Geohazard

This study demonstrates that gas-related processes can be monitored with OBSs as suggested by several studies (e.g., Franek et al., 2017; Tary et al., 2012; Tsang-Hin-Sun et al., 2019). Although the current state of the art does not allow the quantification of the emitted flow rate nor the precise location of the cold seep, OBSs provide convenient means to continuously monitor large areas of seafloor. Indeed, gas fluxes are highly variable in time (Sultan et al., 2011), and acoustic techniques, although valuable, mostly give snapshots, which might not represent the long-term behavior of the seeps. Networks of OBSs could thus be used as a complementary tool to estimate the amount and variability of gas released from the seafloor over wide areas and longer periods.

Monitoring methane or other gas flux is crucial for geohazard assessment in different contexts. In the seismic gap of the SoM, thermogenic and biogenic methane is widespread and the relationship between seismicity and gas has been broadly surveyed since the devastating 1999 Izmit earthquake (e.g., Dupré et al., 2015; Embriaco et al., 2014; Gasperini et al., 2012; Géli et al., 2008). Indeed, areas of gas seepage in the SoM are closely linked to the tectonic regime; in tectonically active sections of the SoM gas migration is driven by the faults and fractures network whereas aseismic segments lack gas emissions (Dupré et al., 2015). Locally strong earthquakes are able to destabilize the gas-rich shallow sediments, as shown by the very shallow aftershocks (Géli et al., 2018) and trigger gas release (Kuşçu et al., 2005) and conduit opening (Tsang-Hin-Sun et al., 2019). In this context, understanding the distribution and evolution of gas-related processes in close relationship with ground motion is crucial for geohazard assessment in the SoM.

Large subduction earthquakes have been proposed to trigger hydrate destabilization and gas discharged into the water column even decades after the earthquake (Fischer et al., 2013). In the case of the 2010 Maule earthquake offshore Chile, high methane concentrations were observed after the mainshock in the water column (Geersen et al., 2016), indicating that the ground motion triggered gas migration. The network of OBSs was installed 5 months after the earthquake, which might be too long to fully characterize the possible relationship between ground motion and gas migration in the marine sediments. During the 3 weeks of the experiments, although many earthquakes occurred, none could be associated with a significant increase in the number of SDEs (see supporting information figure). The relationship between seismicity and gas released is not systematic and depends on many factors, including the seismic energy received, the connection to the source of gas, and local azimuthal effects (e.g., Römer et al., 2017; Figure 9).

Methane constitutes a large part of gas hydrates and free gas found in the SoM or offshore Chile but is also a powerful greenhouse gas with a warming potential that is about 30 times greater than that of carbon dioxide (Intergovernmental Panel on Climate Change, 2014). Therefore, monitoring fluxes of free methane, and more generally gas hydrates, in the marine environment remains important to estimate a global gas budget. On the other hand, the characterization of gas hydrate reservoirs will play a key role in the energy resources landscape in the years to come.

Acknowledgments
We would like to thank the LabexMer Brest for providing funding for the Molene project. The data from the SoM were collected within the MARMARA-DM Demonstration mission of the ESONET (European Seas Observatory NETwork) NOE supported by the 7th Framework Programme (FP7) of the EU. Special acknowledgments to Jean-Françoys Rolin (Ifremer) and Roland Person (Ifremer), coordinators of ESONET and to Namik Cagatay (ITU), Pierre Henry (Cerege), and co-PIs of Marmara-DM. The Istanbul Technical University (ITU) provided R/V Yunuz and long-term valuable support for the operation at sea. Support was provided by the bilateral ANR/TÜBITAK collaborative research project MAREGAMI (ANR-16-CE03-0010-02 and TÜbitak Project 116Y371). Many thanks to Achilles Castelano has work on the SoM data during his Masters project. We would like to thank Nadine Lanteri and Pascal Pelleau for making the deployment of an ocean-bottom seismometer in front of the EMSO-Molène observatory possible. Also, we would like to thank Axel Ehrhold for sharing high-resolution seismic data offshore Molène with us. Marc-André Gutscher is acknowledged for help with the English language. The GMT (Wessel & Smith, 1998) and Seismic Unix software package (Stockwell, 1999) and Qgis software (https://www.qgis.org/fr/site/forusers/download.html) were used in the preparation of several figures in this paper. The ObsPy software was used for processing of the seismic data (Beyreuther et al., 2010) and the Seismic Unix package for plotting the seismic data (Stockwell, 1999). Special thanks are due to Steven Cande and Stephen Lewis, who acquired the openly available data (http://www.ig.utexas.edu/sdc/) of R/V Robert Conrad Cruise RC 2901 (Bangs et al., 1993; Bangs & Cande, 1997; Christeson et al., 2017). E. B., E. T. S. H., C. M., and G. B. worked on the different seismological data sets. F. K., E. C., J. Y. L., and D. D. undertook the fish tank tests. L. G. and F. K. organized the deployment of two seismometers in Molène, L. G. the deployments in the Sea of Marmara, and J. Y. L. and F. K. in the Chile subduction zone. E. B., E. T. S. H. and F. K. drafted the manuscript, and all coauthors read and approved it. Data The seismic data and photos of the EMSO Molene observatory and two associated marine seismometer deployments can be downloaded at the websites (http://doi.org/10.17882/48840 and http://doi.org/10.17882/49245). The seismological data of the Marmara sea ocean-bottom seismometer deployments can be downloaded online

References

Acevedo, J., O'Grady, M., & Wallis, B. (2012). Sighting of the fin whale in the Eastern Subtropical South Pacific: Potential breeding ground? *Revista de Biología Marina y Oceanografía*, *47*(3), 559–563. https://doi.org/10.4067/S0718-19572012000300017

Algar, C. K., Boudreau, B. P., & Barry, M. A. (2011a). Initial rise of bubbles in cohesive sediments by a process of viscoelastic fracture. *Journal of Geophysical Research*, *116*, B04207. https://doi.org/10.1029/2010JB008133

Algar, C. K., Boudreau, B. P., & Barry, M. A. (2011b). Release of multiple bubbles from cohesive sediments. *Geophysical Research Letters*, *38*, L08606. https://doi.org/10.1029/2011GL046870

Auffret, Y., Pelleau, P., Klingelhoefer, F., Geli, L., Crozon, J., Lin, J. Y., & Sibuet, J. C. (2004). MicrOBS: A new generation of ocean bottom seismometer. *First Break*, *22*(1014), 41–47. https://doi.org/10.3997/1365-2397.2004012

Bangs, N. L., & Cande, S. C. (1997). Episodic development of a convergent margin inferred from structures and processes along the southern Chile margin. *Tectonics*, *16*(3), 489–503. https://doi.org/10.1029/97TC00494

Bangs, N. L., Sawyer, D. S., & Golovchenko, X. (1993). Free gas at the base of the gas hydrate zone in the vicinity of the Chile triple junction. *Geology*, *21*(10), 905–908. https://doi.org/10.1130/0091-7613(1993)021<0905:FGATBO>2.3.CO;2

Bayrakci, G., Scalabrin, C., Dupré, S., Leblond, I., Tary, J. B., Lanteri, N., et al. (2014). Acoustic monitoring of gas emissions from the seafloor. Part II: A case study from the Sea of Marmara. *Marine Geophysical Research*, *35*, 211–229. https://doi.org/10.1007/s11001-014-9227-7

Beyreuther, M., Barsch, R., Krischer, L., Megies, T., Behr, Y., & Wassermann, J. (2010). ObsPy: a Python toolbox for seismology. *Seismological Research Letters*, *81*(3), 530–533. https://doi.org/10.1785/gssrl.81.3.530

Boudreau, B. P. (2012). The physics of bubbles in surficial, soft, cohesive sediments. *Marine and Petroleum Geology*, *38*(1), 1–18. https://doi.org/10.1016/j.marpetgeo.2012.07.002

Boudreau, B. P., Algar, C., Johnson, B. D., Croudace, I., Reed, A., Furukawa, Y., et al. (2005). Bubble growth and rise in soft sediments. *Geology*, *33*(6), 517–520. https://doi.org/10.1130/G21259.1

Bourry, C., Chazallon, B., Charlou, J. L., Donval, J. P., Ruffine, L., Henry, P., et al. (2009). Free gas and gas hydrates from the Sea of Marmara, Turkey: Chemical and structural characterization. *Chemical Geology*, *264*(1-4), 197–206. https://doi.org/10.1016/j.chemgeo.2009.03.007

Bowman, D. C., & Wilcock, W. S. (2014). Unusual signals recorded by ocean bottom seismometers in the flooded caldera of Deception Island volcano: volcanic gases or biological activity? *Antarctic Science*, *26*(3), 267–275. https://doi.org/10.1017/S0954102013000758

Buskirk, R. E., Frohlich, C., Latham, G. V., Chen, A. T., & Lawton, J. (1981). Evidence that biological activity affects ocean bottom seismograph recordings. *Marine Geophysical Researches*, *5*(2), 189–205.

Chang, E. T. Y., Chao, B. F., Chen, G.-Y., & Liau, J.-M. (2016). Internal tidesrecorded at ocean bottom off the coast of Southeast Taiwan. *Journal of Geophysical Research: Oceans*, *121*, 3381–3394. https://doi.org/10.1002/2015JC011370

Chouet, B. (1988). Resonance of a fluid-driven crack: Radiation properties and implications for the source of long-period events and harmonic tremor. *Journal of Geophysical ResearchResearch*, *93*(B5), 4375–4400. https://doi.org/10.1029/JB093iB05p04375

Chouet, B. A. (1996). New methods and future trends in seismological volcano monitoring. In *Monitoring and mitigation of volcano hazards*, (pp. 23–97). Berlin, Heidelberg: Springer. https://doi.org/10.1007/978-3-642-80087-0_2

Christeson, G., Shipley, T., Gahagan, L., Johnson, K., & Davis, M. (Eds.) (2017). *Academic Seismic Portal (ASP) at UTIG*. Austin, TX: University of Texas Institute for Geophysics. http://wwwudc.ig.utexas.edu/sdc/

Diaz, J., Gallart, J., & Gaspà, O. (2007). Atypical seismic signals at the Galicia Margin, North Atlantic Ocean, related to the resonance of subsurface fluid-filled cracks. *Tectonophysics*, *433*(1-4), 1–13. https://doi.org/10.1016/j.tecto.2007.01.004

Dupré, S., Scalabrin, C., Grall, C., Augustin, J. M., Henry, P., Şengör, A. C., et al. (2015). Tectonic and sedimentary controls on widespread gas emissions in the Sea of Marmara: Results from systematic, shipborne multibeam echo sounder water column imaging. *Journal of Geophysical Research: Solid Earth*, *120*, 2891–2912. https://doi.org/10.1002/2014JB011617

Embriaco, D., Marinaro, G., Frugoni, F., Giovanetti, G., Monna, S., Etiope, G., et al. (2014). Monitoring of gas and seismic energy release by multiparametric benthic observatory along the North Anatolian Fault in the Sea of Marmara (NW Turkey). *Geophysical Journal International*, *196*(2), 850–866. https://doi.org/10.1093/gji/ggt436

Fischer, D., Mogollón, J. M., Strasser, M., Pape, T., Bohrmann, G., Fekete, N., et al. (2013). Subduction zone earthquake as potential trigger of submarine hydrocarbon seepage. *Nature Geoscience*, *6*(8), 647–651. https://doi.org/10.1038/NGEO1886

(https://doi.org/10.17882/49656 and https://doi.org/10.17882/49764). The Chile seismological data are available at the SEANOE website (https://www.seanoe.org/data/00502/61336/).

Franek, P., Plaza-Faverola, A., Mienert, J., Buenz, S., Ferré, B., & Hubbard, A. (2017). Microseismicity linked to gas migration and leakage on the Western Svalbard Shelf. *Geochemistry, Geophysics, Geosystems*, *18*, 4623–4645. https://doi.org/10.1002/2017GC007107

Gasperini, L., Polonia, A., del Bianco, F., Etiope, G., Marinaro, G., Favali, P., et al. (2012). Gas seepage and seismogenic structures along the North Anatolian Fault in the eastern Sea of Marmara. *Geochemistry, Geophysics, Geosystems*, *13*, Q10018. https://doi.org/10.1029/2012GC004190

Geersen, J., Scholz, F., Linke, P., Schmidt, M., Lange, D., Behrmann, J. H., et al. (2016). Fault zone controlled seafloor methane seepage in the rupture area of the 2010 Maule earthquake, Central Chile. *Geochemistry, Geophysics, Geosystems*, *17*, 4802–4813. https://doi.org/10.1002/2016GC006498

Géli, L., Henry, P., Grall, C., Tary, J. B., Lomax, A., Batsi, E., et al. (2018). Gas and seismicity within the Istanbul seismic gap. *Scientific Reports*, *8*(1), 6819. https://doi.org/10.1038/s41598-018-23536-7

Géli, L., Henry, P., Zitter, T., Dupré, S., Tryon, M., Çağatay, M. N., et al., & the Marnaut Scientific Party (2008). Gas emissions and active tectonics within the submerged section of the North Anatolian Fault zone in the Sea of Marmara. *Earth and Planetary Science Letters*, *274*(1-2), 34–39. https://doi.org/10.1016/j.epsl.2008.06.047

Grevemeyer, I., Diaz-Naveas, J. L., Ranero, C. R., Villinger, H. W., & Leg, O. D. P (2003). Heat flow over the descending Nazca plate in central Chile, 32°S to 41°S: Observations from ODP Leg 202 and the occurrence of natural gas hydrates. *Earth and Planetary Science Letters*, *213*(3-4), 285–298. https://doi.org/10.1016/S0012-821X(03)00303-0

Grevemeyer, I., & Villinger, H. (2001). Gas hydrate stability and the assessment of heat flow through continental margins. *Geophysical Journal International*, *145*(3), 647–660. https://doi.org/10.1046/j.0956-540x.2001.01404.x

Hsu, S. K., Wang, S. Y., Liao, Y. C., Yang, T. F., Jan, S., Lin, J. Y., & Chen, S. C. (2013). Tide-modulated gas emissions and tremors off SW Taiwan. *Earth and Planetary Science Letters*, *369-370*, 98–107. https://doi.org/10.1016/j.epsl.2013.03.013

Intergovernmental Panel on Climate Change (2014). In Core Writing Team, R. K. Pachauri, & L. A. Meyer (Eds.), *Climate Change 2014: Synthesis Report. Contribution of Working Groups I, II and III to the Fifth Assessment Report of the Intergovernmental Panel on Climate Change*, (p. 151). Geneva, Switzerland: IPCC.

Johnson, B. D., Boudreau, B. P., Gardiner, B. S., & Maass, R. (2002). Mechanical response of sediments to bubble growth. *Marine Geology*, *187*(3-4), 347–363. https://doi.org/10.1016/S0025-3227(02)00383-3

Klingelhoefer, F., Pelleau, P., & Geli, L. (2017). Ocean bottom seismometer recording April-June 2016 offshore Molène Island, Brittany, France. SEANOE. https://doi.org/10.17882/49245

Kuşçu, İ., Okamura, M., Matsuoka, H., Gökaşan, E., Awata, Y., Tur, H., et al. (2005). Seafloor gas seeps and sediment failures triggered by the August 17, 1999 earthquake in the eastern part of the Gulf of Izmit, Sea of Marmara, NW Turkey. *Marine Geology*, *215*(3-4), 193–214.

Le Gall, B., Authemayou, C., Ehrhold, A., Paquette, J. L., Bussien, D., Chazot, G., et al. (2014). LiDAR offshore structural mapping and U/Pb zircon/monazite dating of Variscan strain in the Leon metamorphic domain, NW Brittany. *Tectonophysics*, *630*, 236–250. https://doi.org/10.1016/j.tecto.2014.05.026

McDonald, M. A., Hildebrand, J. A., & Webb, S. C. (1995). Blue and fin whales observed on a seafloor array in the Northeast Pacific. *The Journal of the Acoustical Society of America*, *98*(2), 712–721. https://doi.org/10.1121/1.413565

McDonald, M. A., Mesnick, S. L., & Hildebrand, J. A. (2006). Biogeographic characterization of blue whale song worldwide: Using song to identify populations. *Journal of Cetacean Research and Management*, *8*(1), 55–65.

Niu, F., & Li, J. (2011). Component azimuths of the CEArray stations estimated from P-wave particle motion. *Earthquake Science*, *24*(1), 3–13. https://doi.org/10.1007/s11589-011-0764-8

Ostrovsky, A. A. (1989). On the nature of microshocks recorded by ocean bottom seismographs. *Marine Geophysical Researches*, *11*(2), 113–118. https://doi.org/10.1007/BF00285662

Pontoise, B., & Hello, Y. (2002). Monochromatic infra-sound waves recorded offshore Ecuador: Possible evidence of methane release. *Terra Nova*, *14*(6), 425–435. https://doi.org/10.1046/j.1365-3121.2002.00437.x

Römer, M., Wenau,, S., Mau, S., Veloso, M., Greinert, J., Schlüter, M., Bohrmann, G. (2017). Assessing marine gas emission activity and contribution to the atmospheric methane inventory: A multidisciplinary approach from the Dutch Dogger Bank seep area (North Sea). *Geochemistry, Geophysics, Geosystems*, *18*, 2617–2633.

Ruffine, L., Fandino, O., Etoubleau, J., Chéron, S., Donval, J. P., Germain, Y., et al. (2012). Geochemical dynamics of the natural-gas hydrate system in the Sea of Marmara, offshore Turkey. In H. Al-Megren (Ed.), *Geochemical dynamics of the natural-gas hydrate system in the Sea of Marmara, Offshore Turkey, Advances in Natural Gas Technology* (pp. 29–56). London, UK: IntechOpen Limited.

Ryan, W. B. F., Carbotte, S. M., Coplan, J., O'Hara, S., Melkonian, A., Arko, R., et al. (2009). Global Multi-Resolution Topography (GMRT) synthesis data set. *Geochemistry, Geophysics, Geosystems*, *10*, Q03014. https://doi.org/10.1029/2008GC002332

Shaffer, G., Salinas, S., Pizarro, O., Vega, A., & Hormazabal, S. (1995). Currents in the deep ocean off Chile (30°S). *Deep Sea Research Part I: Oceanographic Research Papers*, *42*(4), 425–436. https://doi.org/10.1016/0967-0637(95)99823-6

Sohn, R. A., Hildebrand, J. A., Webb, S. C., & Fox, C. G. (1995). Hydrothermal microseismicity at the megaplume site on the southern Juan de Fuca Ridge. *Bulletin of the Seismological Society of America*, *85*(3), 775–786.

Soule, D. C., & Wilcock, W. S. (2013). Fin whale tracks recorded by a seismic network on the Juan de Fuca Ridge, Northeast Pacific Ocean. *The Journal of the Acoustical Society of America*, *133*(3), 1751–1761. https://doi.org/10.1121/1.4774275

Stein, R. S., Barka, A. A., & Dieterich, J. H. (1997). Progressive failure on the North Anatolian fault since 1939 by earthquake stress triggering. *Geophysical Journal International*, *128*(3), 594–604. https://doi.org/10.1111/j.1365-246X.1997.tb05321.x

Stockwell, J. W. (1999). The CWP/SU: seismic Unix package. *Computers & Geosciences*, *25*(4), 415–419. https://doi.org/10.1016/S0098-3004(98)00145-9

Sultan, N., Riboulot, V., Ker, S., Marsset, B., Géli, L., Tary, J. B., et al. (2011). Dynamics of fault-fluid-hydrate system around a shale-cored anticline in deepwater Nigeria. *Journal of Geophysical Research*, *116*, B12110. https://doi.org/10.1029/2011JB008218

Tary, J. B., Geli, L., Guennou, C., Henry, P., Sultan, N., Çağatay, N., & Vidal, V. (2012). Microevents produced by gas migration and expulsion at the seabed: A study based on sea bottom recordings from the Sea of Marmara. *Geophysical Journal International*, *190*(2), 993–1007. https://doi.org/10.1111/j.1365-246X.2012.05533.x

Tsang-Hin-Sun, E., Batsi, E., Klingelhoefer, F., & Géli, L. (2019). Spatial and temporal dynamics of gas-related processes in the Sea of Marmara monitored with ocean bottom seismometers. *Geophysical Journal International*, *216*(3), 1989–2003. https://doi.org/10.1093/gji/ggy535

Ugalde, A., Gaite, B., Ruiz, M., Villaseñor, A., & Ranero, C. R. (2019). Seismicity and noise recorded by passive seismic monitoring of drilling operations offshore the eastern Canary Islands. *Seismological Research Letters*. https://doi.org/10.1785/0220180353

Varas, G., Vidal, V., & Géminard, J. C. (2009). Dynamics of crater formations in immersed granular materials. *Physical Review E*, *79*(2), 021301. https://doi.org/10.1103/PhysRevE.79.021301

Vargas-Cordero, I., Tinivella, U., & Vilar-Muñoz, L. (2017). Gas hydrate and free gas concentrations in two sites inside the Chilean Margin (Itata and Valdivia Offshores). *Energies*, *10*(12), 2154. https://doi.org/10.3390/en10122154

Villar-Muñoz, L., Behrmann, J. H., Diaz-Naveas, J., Klaeschen, D., & Karstens, J. (2014). Heat flow in the southern Chile forearc controlled by large-scale tectonic processes. *Geo-Marine Letters*, *34*(2-3), 185–198. https://doi.org/10.1007/s00367-013-0353-z

Villar-Muñoz, L., Bento, J. P., Klaeschen, D., Tinivella, U., Vargas-Cordero, I., & Behrmann, J. H. (2018). A first estimation of gas hydrates offshore Patagonia (Chile). *Marine and Petroleum Geology*, *96*, 232–239. https://doi.org/10.1016/j.marpetgeo.2018.06.002

Watkins, W. A. (1981). Activities and underwater sounds of fin whales. *The Scientific Reports of the Whales Research Institute*, *33*, 83–117.

Wessel, P., & Smith, W. H. (1998). New, improved version of Generic Mapping Tools released. *Eos, Transactions American Geophysical Union*, *79*(47), 579.